Cherniak and Zakharenkova *Earth, Planets and Space* (2016) 68:136
DOI 10.1186/s40623-016-0506-1

Earth, Planets and Space

LETTER Open Access

High-latitude ionospheric irregularities: differences between ground- and space-based GPS measurements during the 2015 St. Patrick's Day storm

Iurii Cherniak[1,2*] and Irina Zakharenkova[3]

Abstract

We present an analysis of ionospheric irregularities at high latitudes during the 2015 St. Patrick's Day storm. Our study used measurements from ~2700 ground-based GPS stations and GPS receivers onboard five low earth orbit (LEO) satellites—Swarm A, B and C, GRACE and TerraSAR-X—that had close orbit altitudes of ~500 km, and the Swarm in situ plasma densities. An analysis of the rate of TEC index (ROTI) derived from LEO–GPS data, together with Swarm in situ plasma probe data, allowed us to examine the topside ionospheric irregularities and to compare them to the main ionospheric storm effects observed in ground-based GPS data. We observed strong ionospheric irregularities in the topside ionosphere during the storm's main phase that were associated with storm-enhanced density (SED) formation at mid-latitudes and further evolution of the SED plume to the polar tongue of ionization (TOI). Daily ROTI maps derived from ground-based and LEO–GPS measurements show the pattern of irregularities oriented in the local noon–midnight direction, which is a signature of SED/TOI development across the polar cap region. Analysis of the Swarm in situ plasma measurements revealed that, during the storm's main phase, all events with extremely enhanced plasma densities ($>10^6$ el/cm^3) in the polar cap were observed in the Southern Hemisphere. When Swarm satellites crossed these enhancements, degradation of GPS performance was observed, with a sudden decrease in the number of GPS satellites tracked. Our findings indicate that polar patches and TOI structures in the topside ionosphere were predominantly observed in the Southern Hemisphere, which had much higher plasma densities than the Northern Hemisphere, where SED/TOI structures have already been reported earlier. LEO–GPS data (ROTI and topside TEC) were consistent with these results.

Keywords: Topside ionosphere irregularities, Geomagnetic storm, GPS, ROTI, SED, TOI, Polar patch

Background

Global navigation satellite systems (GNSSs), such as GPS and GLONASS, have become a very powerful and well-proved tool for ionosphere diagnostics, both in quiet and in disturbed geomagnetic conditions, because of their global, continuous and permanent measurements and expanding networks of ground-based receivers. As ionospheric plasma irregularities produce phase and amplitude scintillations of a received radio signal, the GNSS/GPS technique offers a relatively cheap and high-resolution method for tracking these irregularities and permanently monitoring them on a regional and global scale (e.g., Pi et al. 1997; Aarons and Lin 1999; Valladares et al. 2004; Jakowski et al. 2012; Cherniak et al. 2014).

The most intense ionospheric irregularities in the high-latitude ionosphere are caused by plasma processes associated with auroral activities, attributed to auroral particle precipitation, and dynamical processes including high-speed plasma convection (e.g., Phelps and Sagalyn 1976; Fejer and Kelley 1980; Keskinen and Ossakow 1983). The steep ionospheric density gradients and irregularities associated with auroral and cusp precipitation

*Correspondence: tcherniak@ukr.net
[1] Space Weather Laboratory, Kharkiv, Ukraine
Full list of author information is available at the end of the article

in the high latitude cause phase and amplitude fluctuations of GPS signals and have extensively been studied using ground-based GPS data (Skone and Cannon 1995; Mitchell et al. 2004; Alfonsi et al. 2011; Watson et al. 2011; Jiao et al. 2013; Prikryl et al. 2013, 2014; Tiwari et al. 2013; Cherniak et al. 2014; Jacobsen and Andalsvik 2016). However, there are still several unresolved limitations associated with ground-based GPS monitoring of ionospheric irregularities. Firstly, there is a relative scarcity of GPS stations, particularly in the Southern Hemisphere, over oceans, and difficult terrain such as the mainland of Greenland or Antarctica. Secondly, if we use only ground-based GPS data, it is difficult to determine the altitudinal range where the observed ionospheric irregularities occur and develop. These limitations mean that ground-based GPS observations cannot be used to answer the questions of when and where high-latitude topside ionospheric plasma irregularities are developed, or the physical mechanisms of their origin.

One possible solution to these problems is to combine ground-based GPS data with space-borne measurements. Observations from a GPS receiver with a zenith-looking antenna placed onboard a low earth orbit (LEO) satellite offer an opportunity to separate the ionospheric irregularities registered above a LEO from that on the ground. Earlier, Noja et al. (2013), and Zakharenkova and Astafyeva (2015) demonstrated that space-borne GPS measurements onboard a solo-satellite mission (CHAMP) could successfully be used to study the occurrence of high-latitude topside ionospheric irregularities. In this paper, we demonstrate the advantages of using LEO multi-satellite missions for monitoring high-latitude ionospheric irregularities. Our focus was on the successful European Space Agency (ESA) Swarm mission, launched in November 2013, and currently in orbit for more than 2 years. Swarm is a constellation of three identical satellites that orbit at two altitudes of ~460 and ~510 km; the upper satellite (Swarm B) slowly separates in local time from the tandem satellites (Swarms A and C). We analyze the differences in the spatial distribution of ionospheric irregularities detected by the ground-based permanent GPS network with that of the topside GPS measurements onboard the Swarm constellation, using a case study of the 2015 St. Patrick's Day storm. Additionally, we include GPS measurements from Gravity Recovery and Climate Experiment (GRACE) and TerraSAR-X (SAR—synthetic aperture radar) satellites that orbit at similar altitudes to Swarm.

Data and methods

Ground-based GPS measurements

Our approach is based on the analysis of carrier phase delays in the dual-frequency GPS signals when they pass through ionospheric plasma. Pi et al. (1997) introduced two indices for ground-based GPS observations: ROT and ROTI. ROT (rate of TEC (ionospheric total electron content) change) is the time derivative of TEC and is considered to be a measure of phase fluctuation activity. ROT is determined by taking the ratio of the difference between slant TEC values at two successive times to the time interval. ROT is calculated for each visible GPS satellite over a ground-based GPS station in units of TECU/min, where 1 TECU $= 10^{16}$ el/m^2. ROTI (rate of TEC index), a standard deviation of ROT, measures the irregular structure of TEC spatial gradients and is used to characterize the severity of GPS phase fluctuations and detect the presence of ionospheric irregularities. Here, we used a single-layer model that was based on the assumption that all concentrations of electrons are located in an infinitely thin spherical shell at 350 km height; locations of the fluctuations are related to ionosphere piercing points. In our case study of the 2015 St. Patrick's Day storm, we used ground-based GPS stations located in the mid- and high latitudes, with ~2500 and ~180 in the Northern and Southern Hemispheres, respectively. All raw GPS data were resampled to 30 s resolution, with a cutoff elevation angle of 30°. Detailed description of the ROT/ROTI calculation using ground-based GPS data and results for the March 2015 storm is presented in Cherniak et al. (2015).

Further, we used the results obtained from the multi-site GPS database processing to calculate daily polar maps based on ground-based GPS ROTI values. These maps represent a spatial evolution of the high-latitude irregularities and their linkage with the Earth's magnetosphere (due to the strong connections between the Earth's magnetic field and the ionosphere). The ROTI mapping technique is described in detail in Cherniak et al. (2014). ROTI behavior is represented as a function of magnetic local time (MLT) and corrected magnetic latitude (MLAT) for a specific day. We used the corrected geomagnetic (CGM) coordinates with the Definite/International Geomagnetic Reference Field (DGRF/IGRF) models. Such a polar map represents a daily 00–24 MLT time frame and a grid size of 8 min MLT by 2° MLAT, with the latter covering 50°–90°. ROTI data were binned and averaged in each MLAT-MLT bin; the map resolution is 20 bins along the MLAT axis and 180 bins along the MLT axis. In general, the averaged ROTI value in each bin corresponds to the probability of phase fluctuations in the GPS signal, caused by passing of radio signals through ionospheric irregularities. For diurnal ROTI maps, we averaged and binned all ROTI values collected during the 00–24 UT period of a specific day. Additionally, we analyzed several ROTI maps created with 2 h resolution in the geographical coordinates domain.

LEO GPS measurements

Data from a zenith-looking antenna of a space-borne GPS receiver are used mainly for precise orbit determination (POD) purposes, but here we used them in an implementation of the ROTI mapping approach. This allowed us to reveal differences in the spatial distribution of ionospheric irregularities detected on ground and from altitudes above the ionospheric F2 layer peak. As a primary data source, we used POD GPS measurements from three satellite missions: Swarm, TerraSAR-X and GRACE. All these satellites operate in a close range of 450–550 km in a near polar orbit. The polar orbit is highly important for auroral ionosphere research as it is a region where sparse experimental data were available till now.

The Swarm mission consists of three identical satellites; two of them fly in tandem separated by 1°–1.4° at an orbit altitude of 460 km, and the third satellite has an orbit altitude of 510 km. The mission has a multi-instrument payload, of which we used two instruments: (1) Langmuir plasma probe and (2) an eight-channel dual-frequency GPS receiver with a zenith-looking POD antenna. The number of channels in a GPS receiver corresponds to a maximal number of simultaneous tracking GPS satellites. It is worth noting that Swarm is a multi-satellite mission and is able to provide measurements in different local time sectors simultaneously, especially when separation between the tandem and upper satellites reaches several hours. During our case study, Swarm satellite B was separated from A and C by ~1.6 h in local time.

The GRACE mission is a joint US–German project with the overall objective of obtaining long-term data for global models of the Earth's gravity field. In addition to the main gravimetric payload, GRACE has a GPS receiver onboard that uses up to 12 channels for POD purposes. The satellite has a circular polar orbit with inclination of 89°. Orbit altitude in March 2015 was about 430 km.

TerraSAR-X is a German synthetic aperture radar (SAR) Earth observation satellite, which was launched in June 2007. It has a sun-synchronous dawn–dusk polar orbit with an inclination of 97.5°. Orbit altitude in March 2015 was about 515 km. The satellite has a dual-frequency GPS receiver with two zenith antennas for POD and delivers data with 10 s resolution.

POD GPS measurements from these LEO missions are available with different temporal resolutions: 1 s for Swarm and 10 s for GRACE and TerraSAR-X. To harmonize the GPS data from the different missions, we degraded the Swarm data to a 10-s sampling rate. In order to fix the location of the ROTI results, we used piercing points through a thin layer at a fixed altitude of 600 km. For LEO ROTI mapping, we used the same grid as for the ground-based GPS data: corrected geomagnetic coordinates, grid cells 8 min MLT by 2° MLAT and 00–24 h daily data accumulation. Likewise, the LEO ROTI value of a cell was calculated by averaging all values covered by the cell area.

Joint processing of the GPS POD measurements from the missions allows us to increase effectively the spatial data coverage in both Northern and Southern Hemispheres. Figure 1 illustrates how GPS data derived from all five satellites can cover an area of interest, mid- and high latitude, in both hemispheres. All processed lines of sight between LEO and GPS satellites during one full day of March 17, 2015, were recalculated to the MLAT–MLT domain, and MLAT for 40°–90° is accounted.

Figure 1 (first column) shows two polar maps with satellite-to-satellite tracks in MLAT–MLT coordinates when GPS data are available from the Swarms A and C tandem (red and yellow points on the graph). These data covered only morning (06–09 MLT) and evening (18–21 MLT) sectors in both hemispheres. If we add Swarm B data to these polar maps (Fig. 1, second column), the total data coverage is slightly expanded, but still centered in the morning and evening MLT sectors. These projections of the Swarm passes are for mid-March 2015 only, and they are quite different during other months as Swarm has a non-sun-synchronous orbit.

When data from GRACE and TerraSAR satellites are added (next two columns of Fig. 1), we can see that these two satellites flew practically in the same MLT sector, but the total data coverage is expanded as their tracks are nearly perpendicular to the Swarm ones. Finally, GPS data derived from five LEO satellites can cover a wide sector, from morning (08 MLT) practically to noon (11 MLT), and from afternoon (16 MLT) up to midnight (23 MLT). It is important to note that, for the MLAT range of 60°–90°, we have LEO–GPS data for nearly the whole day (00–24 MLT), with better data covering in the Southern Hemisphere. As such, this represents a new data source with ample measurements over polar regions where no or very sparse ground-based GPS measurements exist.

March 2015 geomagnetic storm

The 2015 St. Patrick's Day storm occurred on March 17, 2015, and caused a dramatic response in the ionosphere–plasmasphere–magnetosphere system. To date, it is the strongest geomagnetic storm in 2 years of Swarm operation. The space weather conditions during the event are detailed in several recent papers (Kamide and Kusano 2015; Liu et al. 2015a; Zhang et al. 2015; Cherniak et al. 2015; Jacobsen and Andalsvik 2016). Figure 2 shows the variations in selected interplanetary magnetic field (IMF) and geomagnetic parameters during March 15–20, 2015. The sudden storm commencement (SSC) was registered at ~0445 UT, and then, there was a rapid drop in the SYM-H index to −226 nT at ~2300 UT, with a couple of

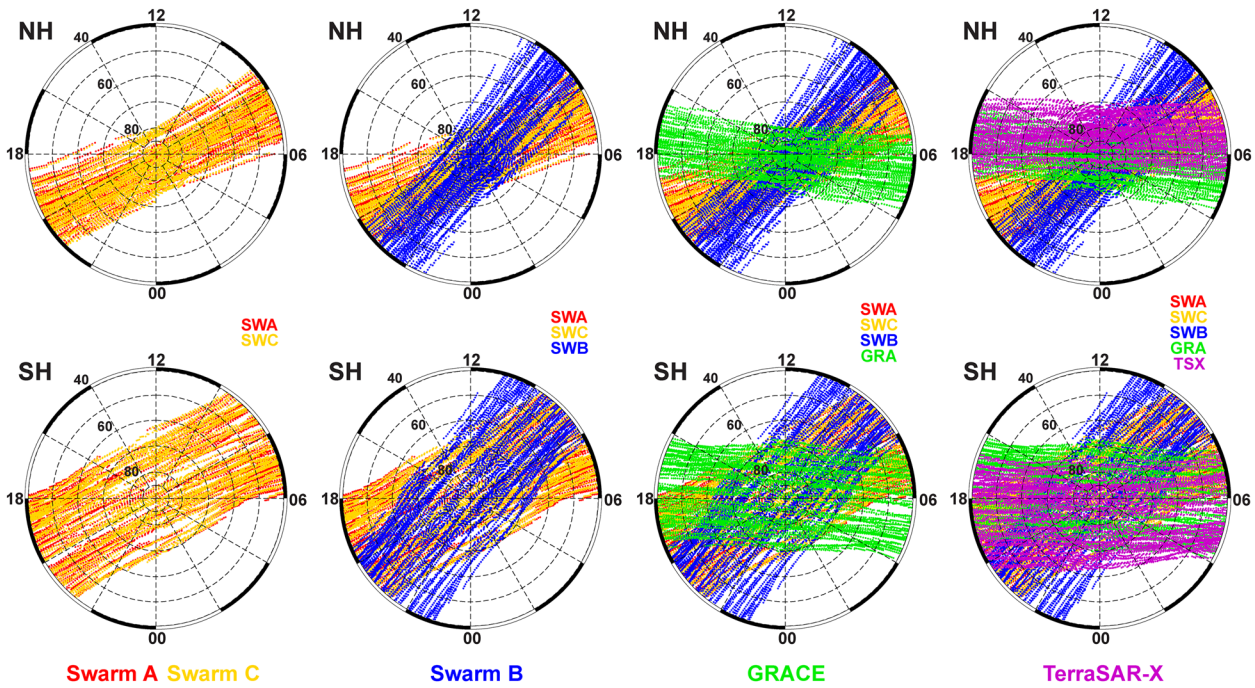

Fig. 1 Projection of LEO–GPS satellite passes recalculated to the MLT–MLAT domain during the full day of March 17, 2015, for the Northern (*top*) and Southern (*bottom*) Hemispheres. *Each row* shows an increase in data coverage (from *left* to *right*) with sequential addition of a satellite to each graph

local minima of −93 and −164 nT at ~0940 and 1740 UT, respectively.

The behavior of the IMF Bz component is shown in Fig. 2 (top panel). After the SSC, the northward IMF Bz component reached a value of ~25 nT. At ~0530 UT, the IMF Bz turned southward and reached the first minimum value of −18 nT at 0615 UT. Then, the IMF Bz turned sharply northward and switched extensively between north and south over ~8 h. After ~1340 UT, the Bz turned southward again and remained southward until the end of the day.

The auroral electrojet index (AE) depicts two intensification peaks at ~09 and 14 UT. Between these two peaks, Bz was observed to turn northward. The mid-latitude magnetic activity index Kp (not shown here) reached a value of 8. The strong disturbance of the geomagnetic field on March 17, 2015, led to intense particle precipitation and an enhancement in substorm activity. It was reported that during March 17–18, 2015, auroras were observed at different locations around the globe, even at mid-latitudes as equatorward as Tasmania and New Zealand in the Southern Hemisphere as well as in the USA, Europe and Japan in the Northern Hemisphere (e.g., Liu et al. 2015b; Kamide and Kusano, 2015; Nishitani et al. 2015; Shiokawa and Otsuka 2015; GUVI TIMED JHU/APL website http://guvitimed.jhuapl.edu, 2015; USGS NGP website http://geomag.usgs.gov/storm/22, 2015 and links therein).

Results

Comparison of ground-based and LEO–GPS diurnal ROTI maps

Figure 3 presents a comparison of diurnal ROTI maps derived from ground-based GPS permanent stations (left column) and LEO–GPS measurement (right column) for the Northern and Southern Hemispheres. The maps are constructed in MLT coordinates. For the quiet day of March 16 (Fig. 3a), the position of the irregularities' oval derived from ground GPS measurements is within 75° MLAT, and ROTI values have their peak intensity around 15 MLT in both hemispheres, associated with dayside cusp precipitation. Intensification of irregularities is also observed within 65°–70° MLAT in the midnight sector for both hemispheres, caused by magnetotail precipitation. However, the LEO ROTI maps do not show intense ionospheric irregularities near and within the auroral region at that time, with an equatorward border around 60° MLAT.

When the main phase of the storm developed, a series of substorms occurred starting at ~06 UT. These substorms resulted in development of enhanced auroral activity and increased visible discrete aurora. As a result,

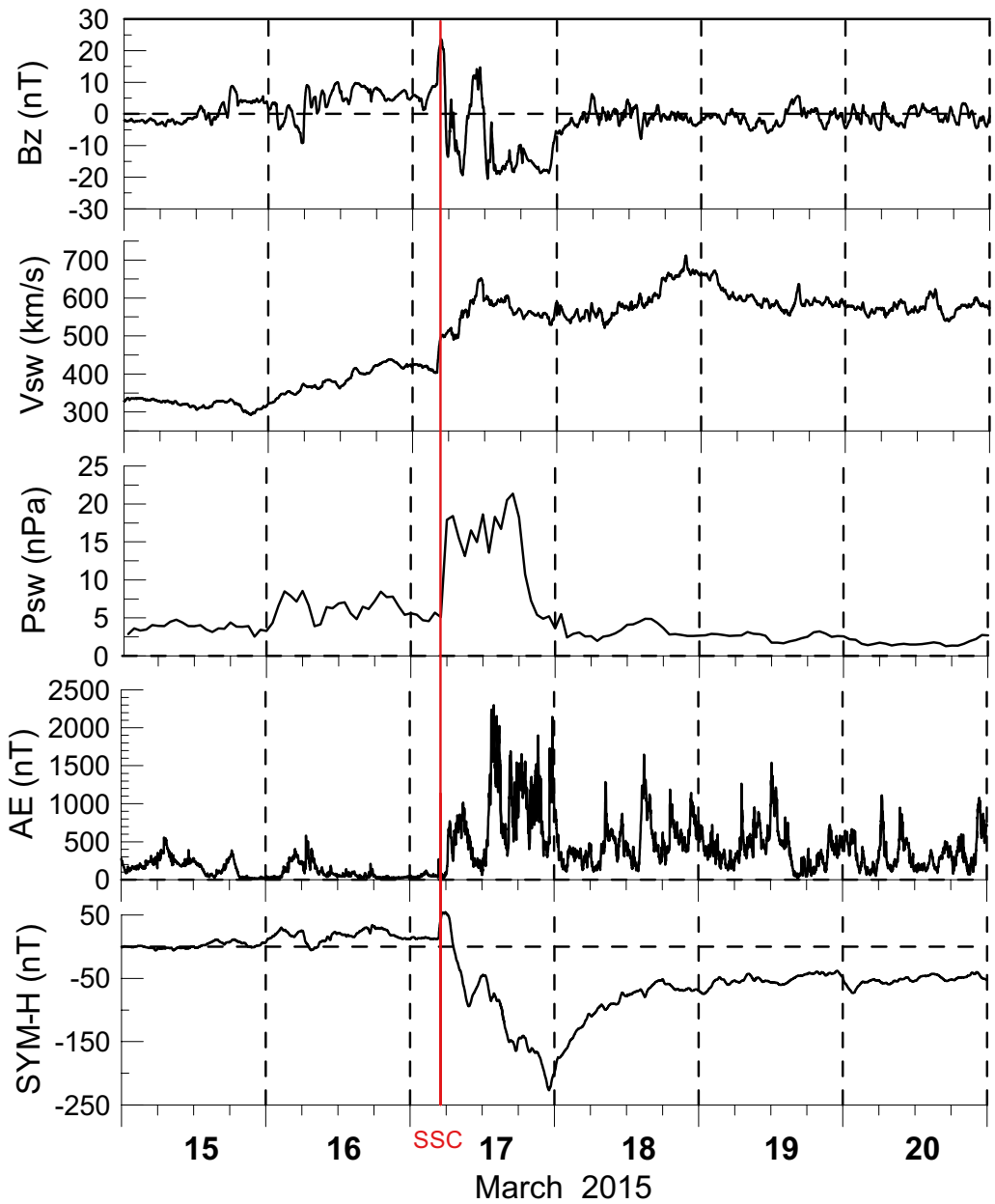

Fig. 2 Variations in the interplanetary magnetic field (IMF) and geomagnetic parameters during March 15–20, 2015. From *top* to *bottom*: IMF Bz component, solar wind speed (Vsw), solar wind ram pressure (Psw), geomagnetic auroral electrojet index (AE) and index of geomagnetic activity (SYM-H). The *red line* indicates the sudden storm commencement (SSC) time (04:45 UT)

persistent strong ionospheric irregularities are registered from ground and above LEO orbit. The daily ROTI map corresponding to the most disturbed day of March 17, 2015 (Fig. 3b), shows dramatic changes in the pattern of high-latitude ionospheric plasma irregularities.

Daily ROTI maps derived from the ground-based GPS data depict a significant increase in ROTI intensity. An oval-like structure of irregularities expands equatorward to ~50° MLAT. A very specific signature of the irregularity pattern is clearly recognized, where intense irregularities are oriented in the day–night direction across the polar cap. This signature is observed in both hemispheres, but with some differences. Over the Northern Hemisphere, the most intense ionospheric irregularities are found within 60°–70° MLAT during ~20–09 MLT, with one noontime peak observed at ~1100–1300 MLT. Distinctly, separate intensity maxima of irregularities can be found within 50°–60° MLAT at ~15–17 MLT.

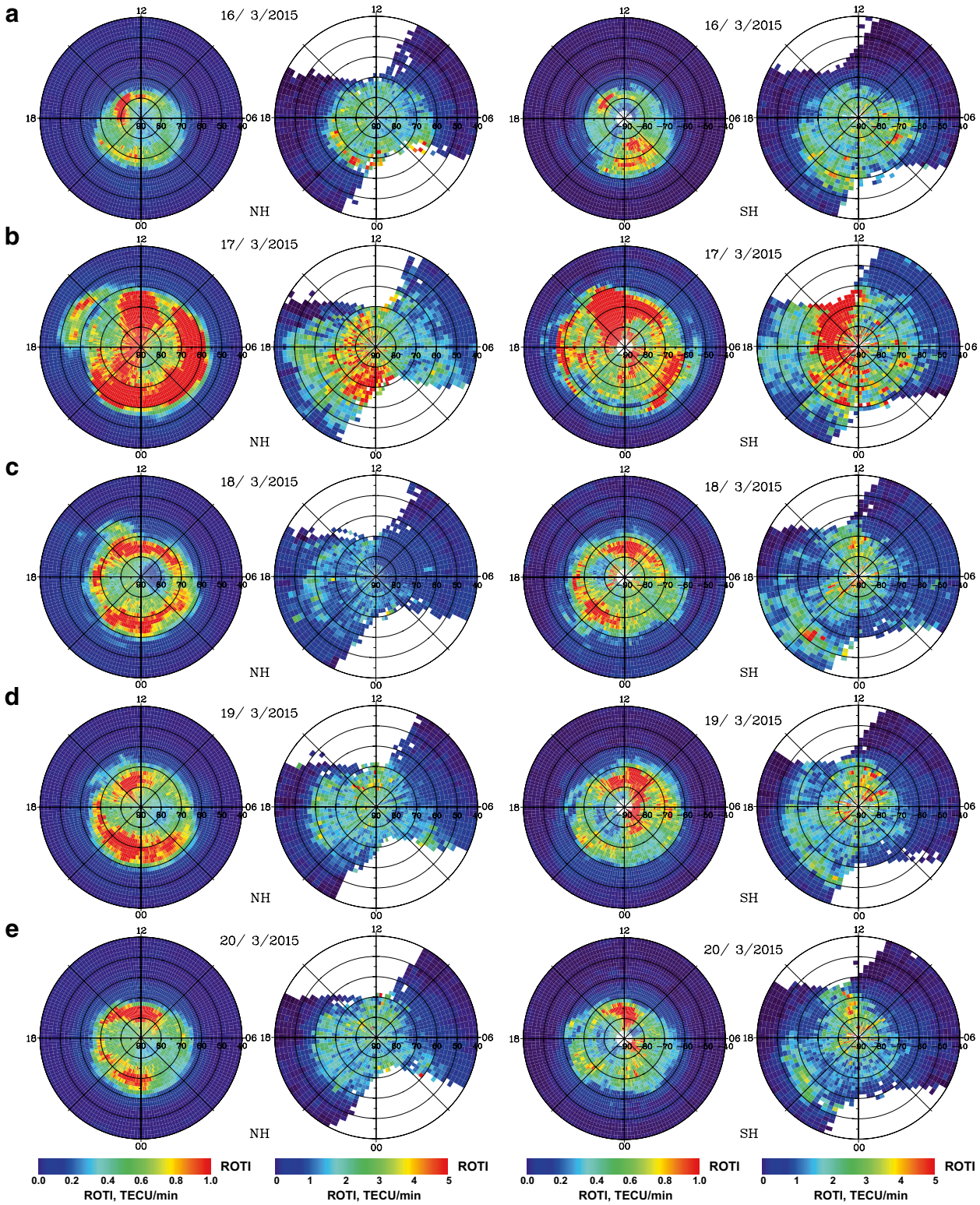

Fig. 3 Diurnal rate of TEC (ionospheric total electron content) index (ROTI) maps derived from ground-based (*first* and *third columns*) and LEO–GPS (*second* and *fourth columns*) measurements for the Northern and Southern Hemispheres (indicated as NH and SH, respectively) during March 16–20, 2015. Horizontal panels (**a**)–(**e**) from top to bottom correspond to the dates of March 16–20, 2015. *Maps* are constructed in corrected geomagnetic coordinates with polar view, covering 00–24 magnetic local time (MLT) and 40°–90° magnetic latitude (MLAT). In *each map*, magnetic noon/midnight is at the *top/bottom*. ROTI is shown in units of TECU/min

In the Southern Hemisphere, there are two intense maxima along the oval: one nighttime maximum at ~04–06 MLT and one in the noon sector at ~09–15 MLT.

Daily ROTI maps derived from LEO–GPS measurements also reveal an equatorward expansion of the ionospheric irregularities with a slight shift to the evening local time (LT) sector, but the strongest and most pronounced irregularities are registered in a day–night direction and oriented over the polar cap. These day–night-oriented irregularities are essentially stronger than an auroral border.

Figure 3c–e shows ionospheric irregularities during the storm recovery phase. The daily ROTI maps (for both ground and LEO–GPS measurements) depict a gradual decrease in irregularity intensity accompanied by a shrinking of the irregularities' oval, but observed ROTI values still exceed the pre-storm ones, especially in ground-based data.

Hourly ROTI maps and in situ Swarm data

Hourly ROTI maps derived from ground-based GPS data were analyzed together with the Swarm in situ electron density (Ne), measured onboard by Langmuir Probe instrument, for the storm's main phase. The results provide qualitative and quantitative characteristics of the ionospheric irregularities detected from ground level and at the altitude of the Swarm satellites. This allows us to examine a possible origin of the irregularities and to study events at ~500 km altitude when Swarm satellites cross polar regions.

Figure 4 shows hourly ROTI maps derived from ground-based GPS data in geographic projections for selected time intervals of March 17, 2015: 04–06, 15–17, 18–20, and 22–24 UT. On each polar map, tracks of Swarm A and Swarm B satellites that passed over during each 2-h interval are superimposed. The corresponding Swarm Ne values are shown along the satellite tracks. These hourly ROTI maps demonstrate the spatial distribution of ionospheric irregularities in a geographic view for the Northern and Southern Hemispheres, covering the period of onset of the geomagnetic storm and three periods during the storm's main phase. It is clear that the Northern Hemisphere has much better GPS data coverage than the Southern, and within the Northern Hemisphere, North America has better data coverage than Asia.

The first pair of the ROTI maps (04–06 UT) shows weak intensity of irregularities in both hemispheres. Swarm Ne variations along satellite tracks reveal plasma density irregularities in the high-latitude region, which is consistent with ground-based observations. The spatial distribution of irregularities dramatically changes during the storm's main phase. The next three ROTI maps for the Northern Hemisphere (Fig. 4, left) represent dynamical changes during three intervals of the main phase. Several significant features are shown in the figures. First, the GPS-detected irregularity oval expanded equatorward, and its equatorial edge was detected in the North American sector at ~50° N latitude. This signature was observed in ground GPS data for more than 6 hours; more detailed description can be found in Cherniak et al. (2015). The second important feature is a radial direction to the distribution of irregularities across the polar cap. Third, the Swarm Ne data depict a noticeable increase in plasma density fluctuations in absolute values compared to that of the 04–06 UT interval. Also, deepening of the main ionospheric trough is seen in the Ne data. The most rapid and intense Ne fluctuations occurred in high latitudes, within the zone of increased intensity of GPS signal fluctuations (ground-based ROTI data).

For the Southern Hemisphere (Fig. 4, right), hourly ROTI maps also demonstrate an increase in intensity of ionospheric irregularities at high latitudes. However, due to substantial sparsity of ground-based GPS stations, it is impossible to determine the location and edges of the irregularity oval as precisely as for the Northern Hemisphere. Superimposed Swarm Ne values can be used to partially restore boundaries of the irregularity oval. But for this case study, the Swarm Ne data reveal another interesting feature in the Southern Hemisphere. For the time interval of 15–17 UT, the absolute values of plasma density fluctuations are much higher in the Southern Hemisphere than in the Northern. In the polar region, several characteristic Ne spikes can clearly be recognized from the low density environment, which can be associated with large-scale polar patches (e.g., Tsunoda 1988). One of the most pronounced Ne increases was detected by Swarm B at 15.8 UT for the latitude range of ~70°–74° S; peak Ne reaches 5.2×10^5 el/cm^3 from the density floor below 1.0×10^5 el/cm^3. However, even more extreme enhancements in Swarm Ne data are found for the next time interval of 18–20 UT. Swarm A and Swarm B satellites both crossed enhanced plasma density structures with peaks of 1.33×10^6 el/cm^3 and 1.67×10^6 el/cm^3, respectively. There are several important points to

(See figure on next page.)

Fig. 4 Hourly rate of TEC (ionospheric total electron content) index (ROTI) maps over the Northern (*left column*) and Southern (*right column*) Hemispheres in geographical projections with superimposed Swarm pass (*thin black line*) and Swarm in situ electron density (Ne) values (*thick black line*) for selected time intervals on March 17, 2015. Geomagnetic poles are marked by *black dots*. SWA and SWB designate Swarm A and Swarm B satellites, respectively. All Swarm Ne data are plotted with the same linear scale

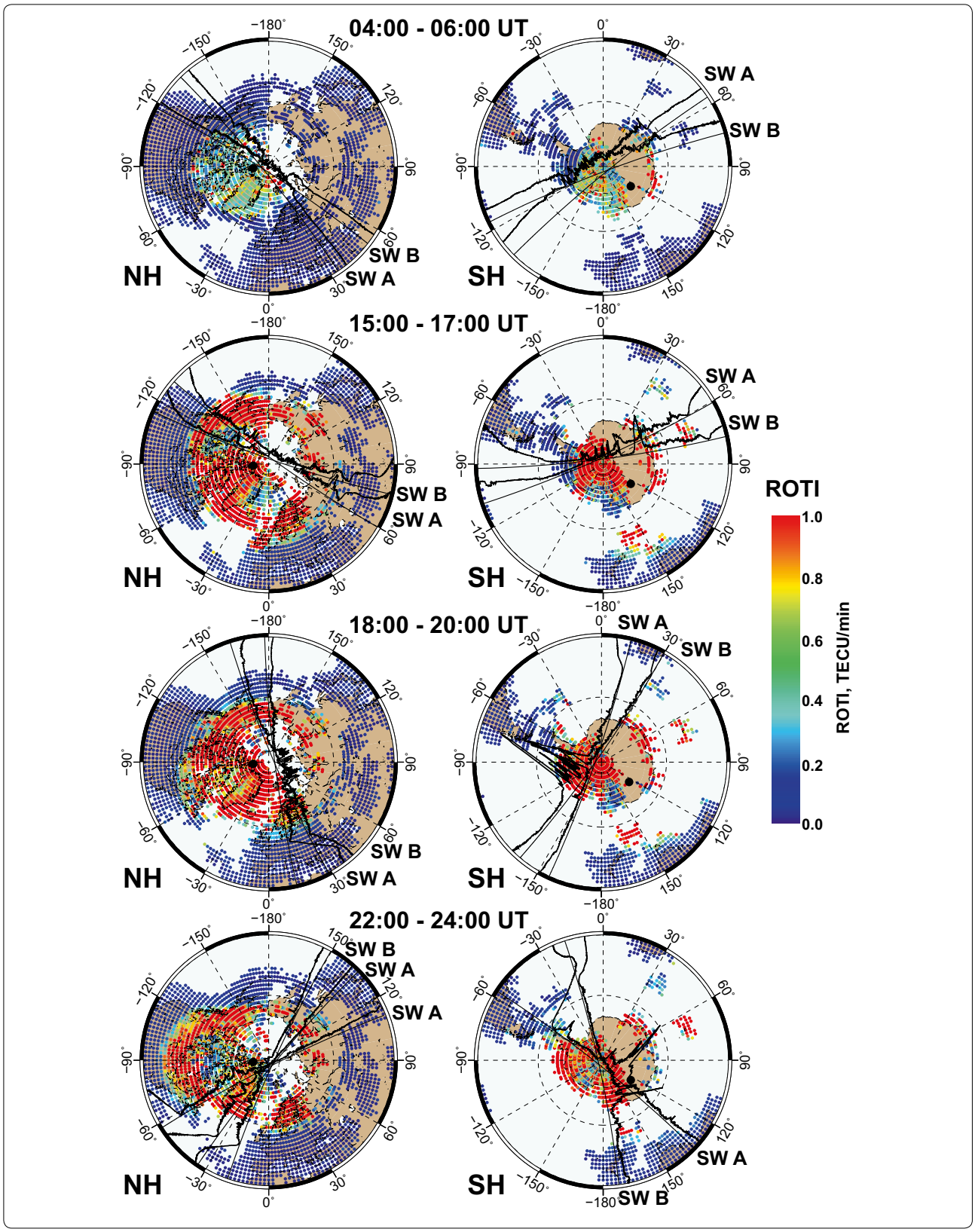
04:00 - 06:00 UT
15:00 - 17:00 UT
18:00 - 20:00 UT
22:00 - 24:00 UT
NH
SH
SW A
SW B
ROTI
ROTI, TECU/min
1.0
0.8
0.6
0.4
0.2
0.0

be emphasized: (1) Such high values of plasma density at an altitude of ~500 km in polar region are quite unusual even during geomagnetic storms; (2) these Ne peaks exceed the surrounding background density of the polar region by 10–15 times; (3) no features of similar magnitude were observed in the Northern Hemisphere during this storm; (4) maximal values of Ne density inside these extreme enhancements are quite comparable with Ne density in the crests of the evening-time equatorial ionization anomaly (19–20 LT) when Swarm satellites crossed it during the day of March 17, 2015, especially prior to 20 UT. Extreme enhancements of electron density, but with lesser magnitude, were also observed in the 22–24 UT interval (Fig. 4, bottom); even these polar region peaks are comparable in absolute values with storm-time Ne enhancement at equatorial and middle latitudes (Swarm A track).

Discussion

In this study, we have compared the pattern of ionospheric irregularities derived from ground-based GPS measurements with daily ROTI maps constructed from multi-satellite LEO–GPS data. We found major differences between the shapes of irregularities' structures observed by these techniques. During the main phase of the March 2015 geomagnetic storm, ground-based ROTI maps indicated that the zone of intense ionospheric irregularities was expanded and moved equatorward comparing to quiescent conditions. The oval pattern of ionospheric irregularities occurred due to plasma density gradients caused by storm-induced particle precipitation and subsequent ionization of the neutral components. We found not only oval patterns of ionospheric irregularities, but also radial structures oriented from the local noon sector to midnight. These structures do not relate to the particle precipitation mechanism and cannot be represented by energetic particle precipitation models.

It is known that radial structures oriented in the day–night direction can be associated with the formation of storm-enhanced density (SED) and further evolution of the SED plume to the polar tongue of ionization (TOI), which follows the convection pattern anti-sunward across the polar cap. Figure 3b confirms the presence of TOI structures in the post-noon sector in both hemispheres, but slightly more intensive in the Southern Hemisphere. SED has been described as a region of enhanced plasma density observed in the post-noon and pre-midnight sectors extending from the equatorward edge of the main ionospheric trough to the noontime cusp (Foster 1993; Coster et al. 2007). The dayside source of the TOI is the SED plume transported from lower latitudes in the post-noon sector by enhanced storm-time electric fields of the subauroral polarization streams (SAPS) (Foster and Burke 2002). The SED latitude decreases with increasing local time and disturbance level (Foster et al. 2005). Anti-sunward convection carries this material through the dayside cusp and across the polar cap to the nightside where the auroral F region is significantly enhanced by the SED material (Foster et al. 2005).

For more detailed study of the SED/TOI appearance during March 17, 2015, in the context of two-cell plasma convection, we compared Super Dual Auroral Radar Network (SuperDARN) polar potential maps with satellite observations. Here, we consider Swarm Ne measurements and two kinds of LEO–GPS observations, topside TEC and ROTI, derived from Swarm, GRACE and TerraSAR-X POD GPS data. To enable visualization of the SuperDARN polar potential maps in the geographic coordinate system, their CGM coordinates were recalculated back to geographic ones.

Figure 5a (left) shows the SuperDARN polar potential map for the Southern Hemisphere at 18.4 UT, with superimposed Swarm A track showing geo-referenced values of electron density and topside ROTI. We observe an extreme enhancement in the Swarm in situ plasma density. We also have two passes with satellite-to-satellite tracking between Swarm A and two GPS satellites (PRN 19 and 21). ROTI values along these passes depict significant increases close to the region with the observed Ne peak. The right-hand panel of Fig. 5a presents detailed variations of electron density (Ne) along Swarm A satellite track, as well as relative TEC for two GPS pass projections. For both GPS satellites, the relative TEC values show a considerable enhancement in magnitude. We should also note that Swarm C, separated from Swarm A by ~10 s in time, shows the same extreme enhancement in electron density as Swarm A. Geographically, all the enhancements identified are located between lobes of the plasma circulation cells on the dayside part of the convection pattern (Fig. 5a, left). But it was not a single event.

(See figure on next page.)

Fig. 5 SuperDARN polar potential maps for the Southern Hemisphere at **a** 18.4 UT and **b** 18.8 UT, and the Northern Hemisphere at **c** 18.0 UT with superimposed low earth orbit (LEO) Rate of TEC (ionospheric total electron content) index (ROTI) (*colored lines*) and in situ (*thick black line*) observations. *Black dot* indicates the position of the magnetic pole. The *right-hand panel* shows Swarm electron density (Ne) and LEO TEC variations for corresponding tracks on the maps. UT and geographic latitude and longitude are noted at the *bottom axes*. Data tracks are line of sight between two points, e.g., "SWA-GPS 19" denotes the data between SWA and GPS PRN 19. TEC data are the relative slant TEC measurements. ROTI is shown in units of TECU/min. Minutes are indicated in *decimal format*

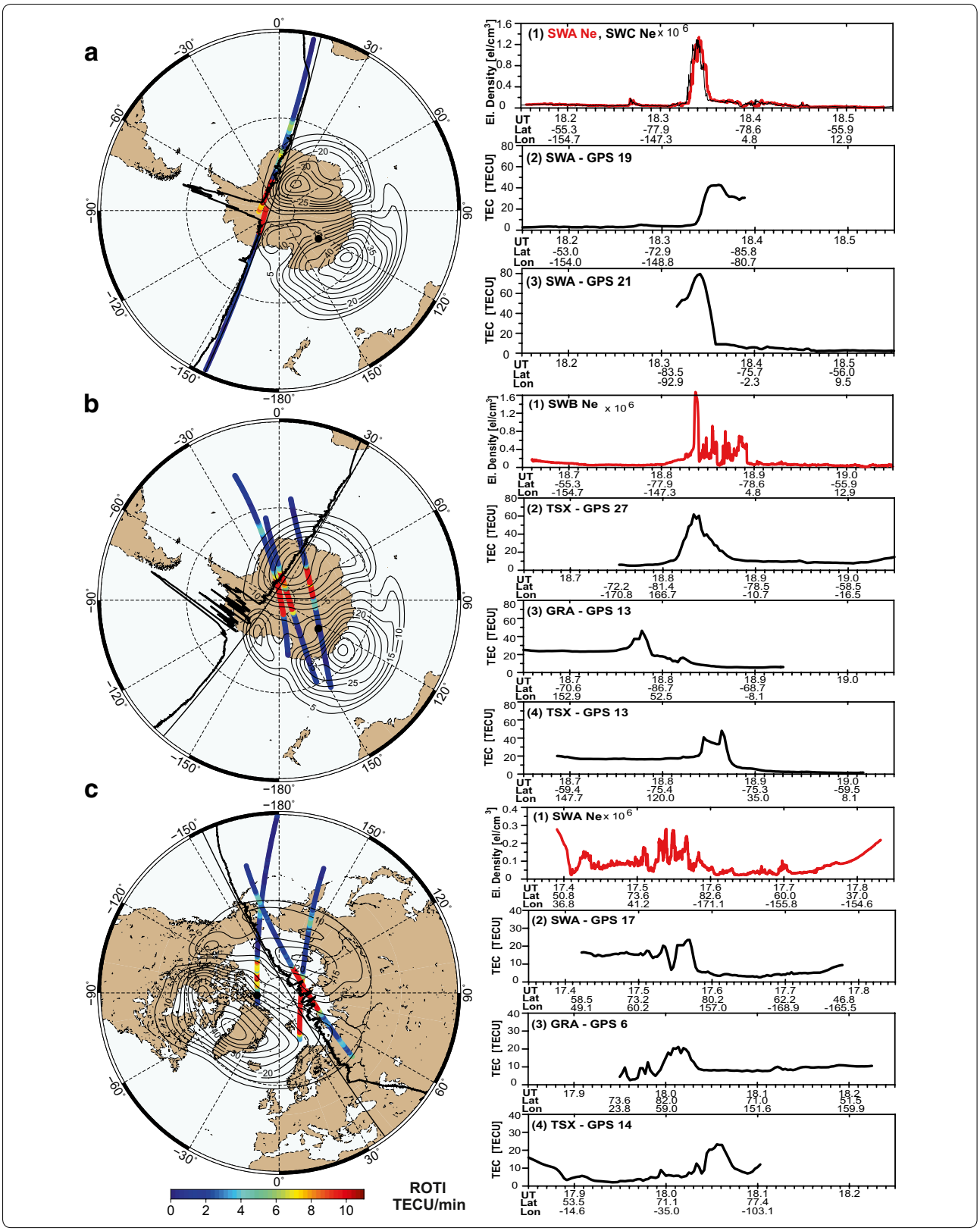
a
b
c
ROTI
TECU/min
0 2 4 6 8 10
(1) SWA Ne, SWC Ne x 10 6
El. Density [el/cm3]
(2) SWA - GPS 19
(3) SWA - GPS 21
TEC [TECU]
UT
Lat
Lon
(1) SWB Ne x 10 6
(2) TSX - GPS 27
(3) GRA - GPS 13
(4) TSX - GPS 13
(1) SWA Ne x 10 6
(2) SWA - GPS 17
(3) GRA - GPS 6
(4) TSX - GPS 14

About half an hour later, Swarm B satellite fortunately passes through the same region and registers a multiple-peak structure in plasma density with a peak value of 1.67×10^6 el/cm^3. This peak density is even higher than that of Swarm A, even despite the fact that the altitude of Swarm B was ~50 km higher (i.e., smaller density might be expected). As is known, when polar patches in the ionospheric F2 region (Tsunoda 1988) are as dense as 10^6 el/cm^3, they cause severe communication/navigation outages when they intersect radio links between receiver and satellite (e.g., Weber and Buchau, 1981; Basu et al. 1988). We should note that while Swarm B crossed these extreme enhancements, there was observed degradation of GPS performance: The number of tracked GPS satellites suddenly decreased from 8 (the maximal number for Swarm GPS receiver) to 0–1. That is the reason we cannot present any collocated GPS tracks for Swarm B satellites. Regarding GPS performance on the Swarm A (C) satellites, a decrease from 8 to 4 (3) tracked GPS satellites was also observed when Swarm crossed this polar patch/TOI structure at 18.35 UT (18:21 UT). Aside from lost Swarm B data, we consider several links to GPS satellites from GRACE and TerraSAR-X. All these GPS tracks are located close to the central part of the two-cell convection pattern, and high ROTI values indicate that they cross large-scale polar patches traveling already from local noon, which was most closely intersected by Swarm B (Ne track), to midnight direction. Significant increases in the topside TEC along these tracks (Fig. 5b, right) reveal that these extreme enhancements, or polar patches, are well developed in the topside ionosphere above ~500 km altitude.

From Fig. 4, we saw that intensity of polar patches in both hemispheres was quite different and Swarm Ne data depicted the dominance of the most intense polar patches in the Southern Hemisphere. Figure 5c shows an example of topside plasma enhancement observed at 18 UT over the Northern Hemisphere. It is clearly seen that observed effects in Ne and TEC are much smaller in magnitude than in the Southern Hemisphere. The Swarm A track crossed the two-cell convection pattern in a different direction, and more rapid and intense Ne fluctuations are observed close to exit to the midnight side. Here, maximal values of plasma density enhancements inside the polar cap are $\sim 0.2 \times 10^6$ el/cm^3, which are quite comparable with the surrounding background density. LEO TEC enhancement observed with Swarm A, GRACE and TerraSAR-X measurements is much lower than in Fig. 5a, b. These topside plasma enhancements are accompanied by strong topside irregularities detected by the LEO ROTI measurements.

We examined all other temporal intervals until 06 UT of March 18 (not shown here) and did not reveal such extreme enhancements in plasma density over the Northern Hemisphere as observed in the Southern. This inter-hemispheric asymmetry can be explained by a strong positive storm effect observed in the Southern Hemisphere in comparison with a negative storm over the North America region (e.g., Astafyeva et al. 2015). The storm-induced plasma enhancement at equatorial and mid-latitudes of South America could support formation of much higher plasma densities in SED/TOI structures (compared with that observed in the Northern Hemisphere) transported toward the Southern polar cap.

Analysis of the combined ground-based GPS and LEO measurements (daily ROTI maps from ground and LEO, 2 h resolution geographical ROTI maps, LEO TEC and in situ electron density) demonstrates that during this particular storm large-scale plasma density enhancements were observed in the topside polar ionosphere of both hemispheres. These enhancements could be most probably associated with SED development and further plasma transportation by subauroral polarization streams in the form of TOI.

We should note that, to date, SED/TOI observations during the March 2015 storm have been reported only for the Northern Hemisphere. Here, we present the first observations of the much more intense SED/TOI structures in the Southern Hemisphere, which were detected mainly due to a fortunate Swarm position.

Another important feature is that the ionospheric SED observed in the Northern Hemisphere during the March 2015 storm was mainly registered above the F2 layer peak (Liu et al. 2015a). Liu et al. (2015a) found that this SED event was identified as a SED in TEC but not in F2 layer peak density NmF2. From Millstone Hill Incoherent Scatter Radar (ISR) measurements, they reported a large increase in electron densities above the F2 peak (>500 km) between 18 and 21 UT, corresponding to the SED passage in TEC over the North American sector. Zhang et al. (2015) studied neutral wind disturbances in subauroral and mid-latitudes during this storm. They observed SED plumes in TEC and ISR electron density enhancements over the northeast US prior to 21 UT before passage of the mid-latitude trough. A strong westward ion drift (500–750 m/s), identified as SAPS, had developed during 21–02 UT, as it was observed by the Millstone Hill ISR. It is worth noting that these SED/TOI structures were well observed in ground-based GPS TEC maps constructed with high spatial resolution (e.g., Liu et al. 2015a; Cherniak et al. 2015).

There are several physical mechanisms for the formation of ionospheric irregularities in the polar ionosphere during TOI development, in particular Kelvin–Helmholtz and gradient-drift instabilities (e.g., van der Meeren et al. 2014). Sojka et al. (1998) discussed one such mechanism

related to plasma motion based on numerical simulation results by the Utah State University Time-Dependent Ionospheric Model. They considered the gradient-drift instability (GDI) as a primary candidate for the generation of these irregularities and showed correlation of GDI with TOI and polar cap patches. They suggested that this mechanism of generating plasma irregularities in the polar ionosphere caused scintillation of transionospheric communication links.

For the March 17, 2015 storm, both factors of the fast neutral and plasma flows, confirmed by the Millstone Hill ISR measurements together with topside plasma enhancement (derived from Swarm LP and topside GPS TEC measurements), support that favorable conditions for GDI development caused the occurrence of the plasma density irregularities in the topside ionosphere.

Recently, Spicher et al. (2015) used Swarm in situ measurements to observe the persistence of more than 90-min kilometer-scale gradients (day and nighttime polar patches) in the Northern polar region. They identified the presence of GDI and obtained GDI growth times using along-track velocities for a test case of December 29, 2013. The maximum magnitude of electron density inside the polar patches was less than 1.4×10^5 el/cm^3. Goodwin et al. (2015) reported on polar patch observation in Swarm Ne data with a top magnitude of ~6.0×10^4 el/cm^3. For the case of the March 2015 storm, we revealed polar patches in the Southern Hemisphere with peak Swarm Ne measurements at least 10 times higher than was observed previously in Swarm data.

Conclusion

Here, we present results of an analysis of GPS measurements, provided by more than 2700 ground-based GPS stations and five LEO satellites, during the March 2015 severe geomagnetic storm. Our main conclusions are:

1. The combined analysis of the rate of TEC index derived from GPS data onboard several LEO satellites (Swarm A, B and C, GRACE and TerraSAR-X) together with Swarm in situ plasma probe data has allowed us to detect topside ionospheric irregularities and to compare them with features of the ionospheric storm's development.
2. The occurrence of strong ionospheric irregularities in the topside ionosphere during the storm's main phase was associated with SED formation at mid-latitudes and further evolution of the SED plume to the polar tongue of ionization.
3. Extreme plasma density enhancements associated with TOI and polar patches were found in the polar cap region of the Southern Hemisphere. They were registered in Swarm Ne data between 15 and 24 UT on March 17, 2015. Maximal Ne densities up to 1.3–1.6×10^6 el/cm^3 (that is 10–15 times higher than the surrounding density level) were observed in the polar region at 18–19 UT.
4. Degradation of GPS performance onboard Swarm satellites was observed when satellites crossed the southern polar cap region, with extreme plasma density enhancements. The number of tracked GPS satellites suddenly decreased from the maximal 8 to 0–4.
5. Analysis of in situ plasma densities measured by the three Swarm satellites demonstrates that during the 2015 St. Patrick's Day storm all polar cap events with extremely enhanced plasma densities that exceeded 10^6 el/cm^3 were observed in the Southern Hemisphere. Moreover, polar patches and TOI structures with lesser densities prevailed also in the Southern Hemisphere and were compared to the Northern Hemisphere, particularly North America, where SED/TOI structures have already been reported (e.g., Liu et al. 2015a). LEO–GPS data (ROTI and topside TEC) confirm these results.
6. During a geomagnetic storm, both types of daily ROTI maps, derived from ground-based and LEO–GPS measurements, could represent the pattern of irregularities oriented in the local noon-midnight direction, which can be considered as an indicator of SAPS and TOI development across the polar cap region.

We conclude that an analysis of concurrent ground-based and LEO–GPS measurements offers a possible way to separate high-latitude ionospheric irregularities caused by direct particle precipitation from those developed due to dynamic plasma processes in the polar ionosphere of both hemispheres. Routine LEO–GPS measurements can provide unprecedented opportunities to further explore this phenomenon and effectively support radar data for solving components of SED/TOI structure modeling.

Authors' contributions

IC designed this study, analyzed the data, and wrote the manuscript. IZ developed software for data processing and helped in interpretation of the data. All coauthors contributed to the revision of the draft manuscript and improvement of the discussion. All authors read and approved the final manuscript.

Author details

[1] Space Weather Laboratory, Kharkiv, Ukraine. [2] Space Radio-Diagnostic Research Center, University of Warmia and Mazury, 2 Oczapowskiego, 10-719 Olsztyn, Poland. [3] Inistitut de Physique du Globe de Paris, 35-39 Rue Helene Brion, 75013 Paris, France.

Acknowledgements

We acknowledge use of the raw GPS data provided by IGS (ftp://cddis.gsfc.nasa.gov), UNAVCO (ftp://data-out.unavco.org), EUREF (ftp://rgpdata.ign.fr), Natural Resources Canada (webapp.geod.nrcan.gc.ca) networks. We acknowledge the European Space Agency (ESA) for providing the Swarm data (http://www.earth.esa.int/swarm) and the Information Systems and Data

Center (ISDC) operated by Geo Forschungs Zentrum Potsdam for GRACE data (http://www.isdc.gfz-potsdam.de/). GPS data from the TerraSAR-X mission are available from the COSMIC Data Analysis and Archive Center (cdaac-http://www.cosmic.ucar.edu/cdaac/). We are grateful to the Virginia Tech SuperDARN Research Group for providing the SuperDARN potential maps (vt.superdarn.org/tiki-index.php?page = ASCIIData). The authors thank the NASA/GSFC's Space Physics Data Facility's OMNIWeb service, for providing OMNI data (ftp://spdf.gsfc.nasa.gov/pub/data/omni) and program code for CGM coordinates calculation. The AE and Kp indices are provided by the World Data Center for Geomagnetism, Kyoto University (wdc.kugi.kyoto-u.ac.jp).

Competing interests

The authors declare that they have no competing interests.

Received: 31 December 2015 Accepted: 6 July 2016
Published online: 30 July 2016

References

Aarons J, Lin B (1999) Development of high latitude phase fluctuations during the January 10, April 10–11, and May 15, 1997 magnetic storms. J Atmos Sol Terr Phys 61:309–327

Alfonsi L, Spogli L, De Franceschi G, Romano V, Aquino M, Dodson A, Mitchell CN (2011) Bipolar climatology of GPS ionospheric scintillation at solar minimum. Radio Sci 46:RS0D05. doi:10.1029/2010RS004571

Astafyeva E, Zakharenkova I, Fцrster M (2015) Ionospheric response to the 2015 St. Patrick's Day storm: a global multi-instrumental overview. J Geophys Res Space Phys 120:9023–9037. doi:10.1002/2015JA021629

Basu S, MacKenzie E, Basu S (1988) Ionospheric constraints on VHF/UHF communications links during solar maximum and minimum periods. Radio Sci 23:363–378. doi:10.1029/RS023i003p00363

Cherniak Iu, Krankowski A, Zakharenkova I (2014) Observation of the ionospheric irregularities over the Northern Hemisphere: methodology and service. Radio Sci 49:653–662. doi:10.1002/2014RS005433

Cherniak Iu, Zakharenkova I, Redmon R (2015) Dynamics of the high-latitude ionospheric irregularities during the March 17, 2015 St. Patrick's Day storm: ground-based GPS measurements. Space Weather 13:585–597. doi:10.1002/2015SW001237

Coster AJ, Colerico MJ, Foster JC, Rideout W, Rich F (2007) Longitude sector comparisons of storm enhanced density. Geophys Res Lett 34(18):L18105. doi:10.1029/2007GL030682

Fejer BG, Kelley MC (1980) Ionospheric irregularities. Rev Geophys Space Phys 18(2):401–454

Foster JC (1993) Storm time plasma transport at middle and high latitudes. J Geophys Res 98(A2):1695

Foster JC, Burke WJ (2002) SAPS: a new categorization for sub-auroral electric fields. EOS Trans AGU 83(36):393–394. doi:10.1029/2002EO000289

Foster JC, Coster AJ, Ericson PJ, Holt JM, Lind FD, Rideout W, McCready M et al (2005) Multiradar observations of the polar tongue of ionization. J Geophys Res 110:A09S31. doi:10.1029/2004JA010928

Goodwin L, Iserhienrhien B, Miles DM, Patra S, van der Meeren C, Buchert SC, Burchill J, Clausen LBN, Knudsen DJ, McWilliams KA, Moen J (2015) Swarm in situ observations of F-region polar cap patches created by cusp precipitation. Res Lett, Geophys. doi:10.1002/2014GL062610

GUVI TIMED JHU/APL website (2015) guvitimed.jhuapl.edu, guvitimed.jhuapl.edu/guvi-images/guvi_aur.gif. Accessed 24 Dec 2015

Jacobsen KS, Andalsvik YL (2016) Overview of the 2015 St. Patrick's Day storm and its consequences for RTK and PPP positioning in Norway. J Space Weather Space Clim 6:9. doi:10.1051/swsc/2016004

Jakowski N, Bйniguel Y, De Franceschi G, Hernбndez-Pajares M, Jacobsen KS, Stanislawska I, Tomasik L, Warnant R, Wautelet G (2012) Monitoring, tracking and forecasting ionospheric perturbations using GNSS techniques. J Space Weather Space Clim 2:A22. doi:10.1051/swsc/2012022

Jiao Y, Morton YT, Taylor S, Pelgrum W (2013) Characterization of high-latitude ionospheric scintillation of GPS signals. Radio Sci 48:698–708. doi:10.1002/2013RS005259

Kamide Y, Kusano K (2015) No major solar flares but the largest geomagnetic storm in the present solar cycle. Space Weather 13:365. doi:10.1002/2015SW001213

Keskinen MJ, Ossakow SL (1983) Theories of high-latitude ionospheric irregularities: a review. Radio Sci 18(6):1077–1091. doi:10.1029/RS018i006p01077

Liu J, Wang W, Burns A, Yue X, Zhang S, Zhang Y, Huang C (2015a) Profiles of ionospheric storm-enhanced density during the 17 March 2015 great storm. J Geophys Res Space Phys 121:727. doi:10.1002/2015JA021832

Liu TC, Shao X, Cao C, Zhang B, Fung SF, Sharma S (2015b) Aurora activities observed by SNPP VIIRS day–night band during St. Patrick's Day, 2015 G4 level geomagnetic storm. AGU Fall Meeting, San Francisco, p SA31D-2360

Mitchell CN, Alfonsi L, De Francesci G, Lester M, Romano V (2004) GPS TEC and scintillation measurements from the polar ionosphere during the October 2003 storm. Geophys Res Lett 32:L12S03. doi:10.1029/2004GL021644

Nishitani N, Hori T, Kataoka R, Ebihara Y, Shiokawa K (2015) Characteristics of ionospheric convection associated with low-latitude aurora observed at Rikubetsu, Hokkaido during the 2015 March storm, paper presented at SuperDARN workshop 2015, Leicester

Noja M, Stolle C, Park J, Lьhr H (2013) Long-term analysis of ionospheric polar patches based on CHAMP TEC data. Radio Sci 48(3):289–301. doi:10.1002/rds.20033

Phelps ADR, Sagalyn RC (1976) Plasma density irregularities in the high-latitude top side ionosphere. J Geophys Res 81(4):515–523. doi:10.1029/JA081i004p00515

Pi X, Mannucci AJ, Lindqwister UJ, Ho CM (1997) Monitoring of global ionospheric irregularities using the worldwide GPS network. Geophys Res Lett 24:2283

Prikryl P, Ghoddousi-Fard R, Kunduri BSR, Thomas EG, Coster AJ, Jayachandran PT, Spanswick E, Danskin DW (2013) GPS phase scintillation and proxy index at high latitudes during a moderate geomagnetic storm. Ann Geophys 31:805–816. doi:10.5194/angeo-31-805-2013Prikryl

Prikryl P, Jayachandran PT, Mushini SC, Richardson IG (2014) High-latitude GPS phase scintillation and cycle slips during high-speed solar wind streams and interplanetary coronal mass ejections: a superposed epoch analysis. Earth, Planets Space 66:62. doi:10.1186/1880-5981-66-62

Shiokawa K, Otsuka Y (2015) Low-latitude red aurora observed in Japan during the St. Patrick's Day 2015 Event. SCOSTEP-WDS workshop on global data activities for the study of solar-terrestrial variability, NICT, Tokyo, 28–30 September 2015. Book of Abstracts. p 34

Skone S, Cannon ME (1995) Ionospheric effects on differential GPS applications during auroral substorm activity. ISPRS J Photogram Remote Sens 54:279–288

Sojka JJ, Subramanium MV, Zhu L, Schunk RW (1998) Gradient-drift instability growth rates from global scale modeling of the polar ionosphere. Radio Sci 33(6):1915–1928

Spicher A, Cameron T, Grono EM, Yakymenko KN, Buchert SC, Clausen LBN, Knudsen DJ, McWilliams KA, Moen J (2015) Observation of polar cap patches and calculation of gradient drift instability growth times: a Swarm case study. Geophys Res Lett 42:201–206. doi:10.1002/2014GL062590

Tiwari R, Strangeways HJ, Tiwari S, Ahmed A (2013) Investigation of ionospheric irregularities and scintillation using TEC at high latitude. Adv Space Res 52:1111–1124. doi:10.1016/j.asr.2013.06.010

Tsunoda RT (1988) High-latitude F region irregularities: a review and synthesis. Rev Geophys 26:719–760

Valladares CE, Villalobos J, Sheehan R, Hagan MP (2004) Latitudinal extension of low-latitude scintillations measured with a network of GPS receivers. Ann Geophys 22:3155–3175. doi:10.5194/angeo-22-3155-2004

van der Meeren C, Oksavik K, Lorentzen D, Moen JI, Romano V (2014) GPS scintillation and irregularities at the front of an ionization tongue in the nightside polar ionosphere. J Geophys Res Space Phys 119:8624–8636. doi:10.1002/2014JA020114

Watson C, Jayachandran PT, Spanswick E, Donovan EF, Danskin DW (2011) GPS TEC technique for observation of the evolution of substorm particle precipitation. J Geophys Res 116:0090. doi:10.1029/2010JA015732

Weber EJ, Buchau J (1981) Polar cap F-455 layer auroras. Geophys Res Lett 8:125–128. doi:10.1029/GL008i001p00125

Zakharenkova I, Astafyeva E (2015) Topside ionospheric irregularities as seen from multisatellite observations. J Geophys Res Space Phys 120(1):807–824. doi:10.1002/2014JA020330

Zhang S, Erickson PJ, Foster JC, Holt JM, Coster AJ, Makela JJ, Noto J, Meriwether JW, Harding BJ, Riccobono J, Kerr RB (2015) Thermospheric poleward wind surge at midlatitudes during great storm intervals. Geophys Res Lett 42:5132–5140. doi:10.1002/2015GL064836